Actomyosin purse strings: renewable resources that make morphogenesis robust and resilient

Alice Rodriguez-Diaz,[1] Yusuke Toyama,[2] Daniel L. Abravanel,[1,3] John M. Wiemann,[1,4] Adrienne R. Wells,[1] U. Serdar Tulu,[1] Glenn S. Edwards,[2] and Daniel P. Kiehart[1]

[1]Department of Biology, Duke University, Durham, North Carolina 27708-0338
[2]Physics Department, Duke University, Durham North Carolina 27708-0319
[3]Current address: School of Medicine, University of Pennsylvania
[4]Current address: Department of Orthopedics, University of New Mexico

(Received 13 March 2008; accepted 16 June 2008; published online 23 July 2008)

Dorsal closure in *Drosophila* is a model system for cell sheet morphogenesis and wound healing. During closure two sheets of lateral epidermis move dorsally to close over the amnioserosa and form a continuous epidermis. Forces from the amnioserosa and actomyosin-rich, supracellular purse strings at the leading edges of these lateral epidermal sheets drive closure. Purse strings generate the largest force for closure and occur during development and wound healing throughout phylogeny. We use laser microsurgery to remove some or all of the purse strings from developing embryos. Free edges produced by surgery undergo characteristic responses as follows. Intact cells in the free edges, which previously had no purse string, recoil away from the incision and rapidly assemble new, secondary purse strings. Next, recoil slows, then pauses at a turning point. Following a brief delay, closure resumes and is powered to completion by the secondary purse strings. We confirm that the assembly of the secondary purse strings requires RhoA. We show that α-actinin alternates with nonmuscle myosin II along purse strings and requires nonmuscle myosin II for its localization. Together our data demonstrate that purse strings are renewable resources that contribute to the robust and resilient nature of closure.
[DOI: 10.2976/1.2955565]

CORRESPONDENCE
Daniel P. Kiehart:
dkiehart@duke.edu

Morphogenesis of epithelial sheets is a common feature of animal development based on highly coordinated cell shape changes and rearrangements. Understanding such movements requires determining how tissue kinematics (the analysis of cell movements) and cellular dynamics (the analysis of the forces that underlie those movements) are organized and regulated in space and time. Mechanical properties of cells, such as stiffness, adhesion, elasticity, and contractility all contribute to the production and transmission of such forces and their impact on tissue and cell kinematics (Keller *et al.*, 2003).

Dorsal closure is a genetically tractable morphogenic process in *Drosophila* (Campos-Ortega and Hartenstein, 1985; Martinez-Arias, 1993; Young *et al.*, 1993; Agnes and Noselli, 1999; Kiehart, 1999; Harden, 2002; Jacinto *et al.*, 2002b). The kinematics of closure are easily visualized in both wild type and genetically altered, living embryos with the use of green fluorescent protein, GFP (e.g., Fig. 1). This allows us to link the genetic program that specifies development in *Drosophila* to force production during morphogenesis. We use targeted laser microsurgery and biophysical reasoning to evaluate the cellular dynamics that produce and transmit forces that drive morphogenesis (Kiehart *et al.*, 2000; Hutson *et al.*, 2003; Homsy *et al.*, 2006; Kiehart *et al.*, 2006; Peralta *et al.*, 2007; Peralta *et al.*, 2008).

HFSP Journal © HFSP Publishing $25.00
Vol. 2, No. 4, August 2008, 220–237 http://hfspj.aip.org

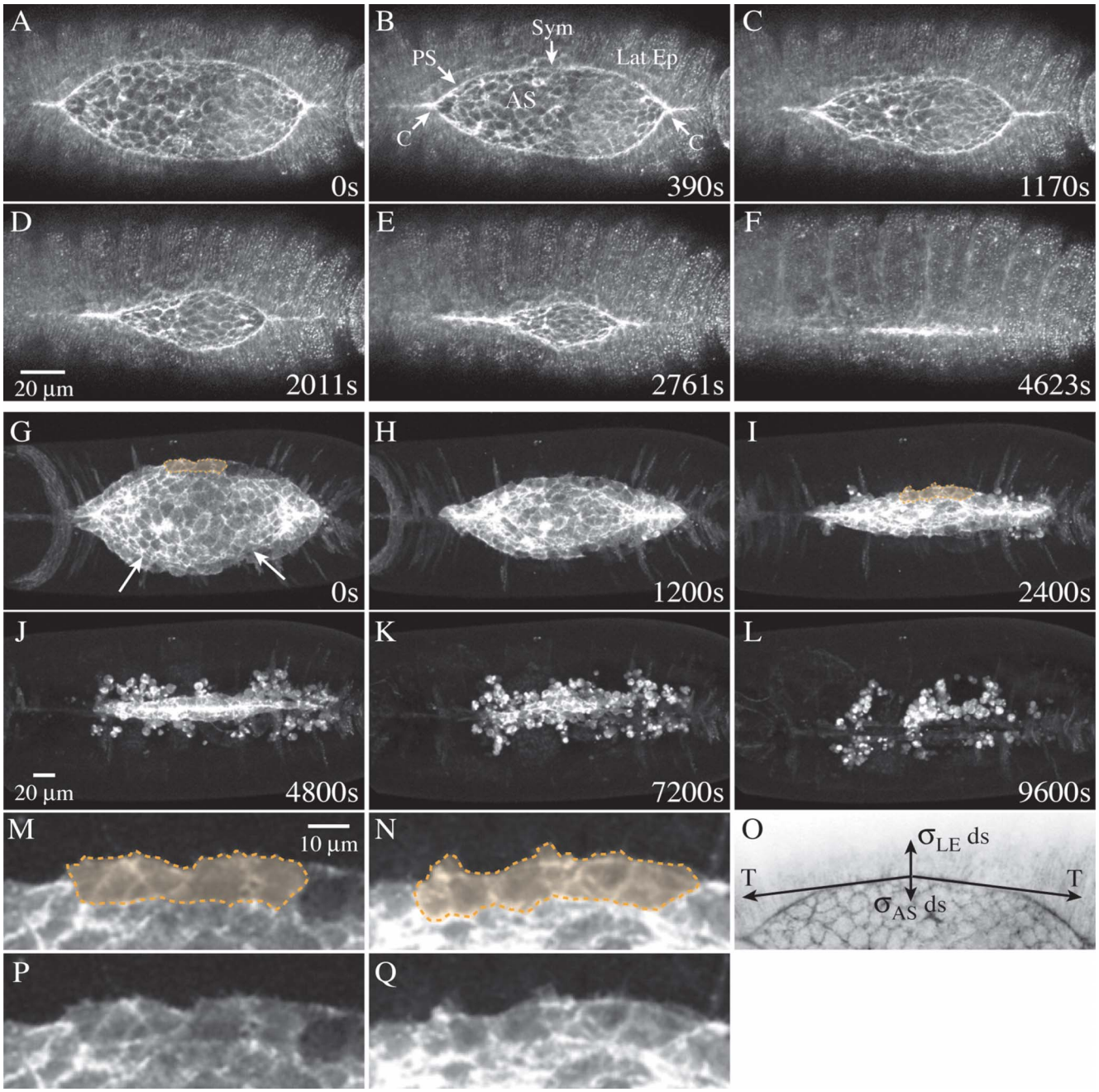

Figure 1. Embryos that express GFP-moe ubiquitously (A–F) or in the amnioserosa alone (G–N) illustrate the kinematics of native closure. (A–F) Confocal micrographs show a native, unperturbed embryo, expressing GFP-moesin to label F-actin. The time stamp of 0 s indicates the first image taken for the given embryo. Structures labeled in B include a purse string (PS), the canthi (C), the symmetry point (Sym), the amnioserosa (AS), and the lateral epidermis (Lat Ep). In F, closure is complete but the supracellular purse string has not yet disappeared (eventually it does). The scale bar in D represents 20 μm and applies to panels A–F. (G–L) A single embryo is expressing GFP-moe in the amnioserosa (c381-GAL4 driver and UAS-GMA responder). Arrows in G show the approximate position of the purse strings in the leading edges of the lateral epidermal cell sheets. Shading in G, I, M and N show the intact row of amnioserosa cells that underlie the lateral epidermis. Closure of the overlying epidermis is close to complete in I when apoptosis begins to cause the bulk of the amnioserosa to disassemble. In J, only the row that had been tucked under the first row of lateral epidermal cells remains intact. In K and L, cell fragments move away from the dorsal midline because macrophage-like hemocytes phagocytose fluorescent remnants of apoptotic amnioserosa cells. M and N are insets corresponding to the areas of underlying amnioserosa shown in panels G and I with shading. Panels P and Q show the same areas of the amnioserosa as shown in M and N, but without shading. The 20 μm scale bar in J is for panels G–L, the 10 μm scale bar in M is for panels M, N, P and Q. Panel O includes a schematic diagram of the forces applied to an infinitesimal segment, *ds*, at the symmetry point (vectors are not drawn to scale).

During closure, which occurs midway through *Drosophila* embryogenesis, the developing embryo becomes fully enclosed by the epidermis [Figs. 1(A)–1(F), see Supplemental Video 1]. At the onset of closure, the dorsal surface of the embryo is covered by the large, flat polygonal cells of the amnioserosa [AS in Fig. 1(B)]. The rest of the embryo is covered by the smaller, cuboidal-to-columnar cells of the lateral [Lat Ep in Fig. 1(B)] and ventral epidermis. The visible area of the amnioserosa has a shape similar to the human eye, with a wide central section that tapers into two canthi, the "corners" of the eye [C in Fig. 1(B)]. In amnioserosa cells, the actin cytoskeleton is largely restricted to a cortical network, enriched at or near apical cell junctions. During early closure, the leading-edge cells (also called the dorsal-most cells of the lateral epidermis) become organized into well defined rows in which actin and nonmuscle myosin II assemble to form supracellular purse strings or actomyosin-rich cables (one on each side of the embryo, Young *et al.*, 1993; Kiehart *et al.*, 2000). Recently, Wada and colleagues showed that the cells of the amnioserosa, where they tightly appose the lateral epidermis, also contain purse string-like structures (Wada *et al.*, 2007).

The leading edge cells form supracellular purse strings or F-actin and nonmuscle myosin II rich cables that are distinct in form from the cortical actomyosin arrays found in most cells. Moreover, these leading edge cells comprise a distinct tissue that overlaps and adheres to the single row of cells of the amnioserosa. Foe (1989) observed that the leading edge cells enter the 14th mitotic division together, thereby constituting a mitotic domain (domain 19). This indicates that they have a common cell fate that is distinct from the fates of other cells on the surface of the embryo.

As dorsal closure proceeds, cells of the participating tissues change shape when their actin cytoskeletons are remodeled. Such movements can be observed by expressing GFP-moe ubiquitously [Figs. 1(A)–1(F), Supplemental Video 1(A)] or in selected tissues [Figs. 1(G)–1(N), 1(P) and 1(Q); Supplemental Video 1(B)]. Eventually, the entire amnioserosa is enclosed within the epidermis and its molecular components are recycled via apoptosis [Figs. 1(I)–1(L), Kiehart *et al.*, 2000]. Note that as the leading edge and the amnioserosa change shape, the relationship between the dorsal most row of lateral epidermal cells, which contain the purse strings, and the first row of amnioserosa cells [shadowed in Figs. 1(G), 1(L), 1(M), and 1(N)] remains nearly constant until the amnioserosa is, with time, disassembled by apoptosis [Figs. 1(I)–1(L)]. Thus, in native closure, the lateral epidermis does not crawl over a substrate comprised of amnioserosa cells. Throughout this manuscript "native" refers to embryos or structures that have not been perturbed by laser interrogation.

Forces for closure are contributed by the leading edge and the amnioserosa (Kiehart *et al.*, 2000; Hutson *et al.*, 2003; Peralta *et al.*, 2007). In contrast forces from the bulk of the lateral epidermis oppose closure. Tension in the supracellular purse strings also contributes forces that maintain a uniform epithelial advance (Kiehart *et al.*, 2000; Bloor and Kiehart, 2002; Jacinto *et al.*, 2002a; Wood *et al.*, 2002; Hutson *et al.*, 2003). Finally, as the two opposing epithelial sheets meet each other at the dorsal midline they suture together. Filopodia and lamellipodia at the leading edge may contribute to this process in a regulatory and/or structural fashion, by mediating adhesive and segment matching processes during dorsal closure (Jacinto *et al.*, 2000; Millard and Martin, 2008). Ultimately, the dorsal surface is covered by a continuous epithelium that appears seamless.

To investigate the relative magnitude of the forces that drive closure, we formalize a force balance equation based on Newton's second law (detailed in Hutson *et al.*, 2003). This dynamical equation is for the symmetry points, which in native closure are equivalent to the points, one on each purse string, that are farthest from the dorsal midline [Sym in Fig. 1(B), Hutson *et al.*, 2003 Fig. 1(O)]. Under the regime of low Reynolds number (Berg, 1983):

$$\sigma_{LE} - \sigma_{AS} - T\kappa = b\ dh/dt. \tag{1}$$

The stress σ_{LE} is the sheet force per unit length applied to the leading edge by the lateral epidermis and the stress σ_{AS} is the sheet force per unit length due to the amnioserosa. T is the tension in the purse string, κ is the curvature of the purse string, thus $T\kappa$ is the stress due to the purse string resolved in the direction of movement toward the dorsal midline. b is the drag coefficient and $b\ dh/dt$ is the viscous drag on the system. At a symmetry point, the stresses σ_{LE}, σ_{AS}, $T\kappa$ and the vector dh/dt are collinear and in the direction along an axis that is perpendicular to the dorsal midline. As a consequence, Eq. (1) can be treated as a scalar equation.

The relative magnitudes of these forces have been described by two "force ladders," which indicate that the tension in the purse string is the largest contributing force (Hutson *et al.*, 2003; Peralta *et al.*, 2007). $\sigma_{LE}:\sigma_{AS}:T\kappa:b\ dh/dt$ ranges in magnitudes from $\sim$510:380:130:1 to $\sim$490:380:110:1 and $T:\sigma_{AS}\Delta s_{AS}:\sigma_{LE}\Delta s_{LE}$ ranges from $\sim$15:3:1 to $\sim$6:3:1. The positions of $T\kappa$ and T in the ordering of the two ladders can be understood by recognizing that the curvature κ is small, i.e., the leading edge forms a shallow arc and the projection of T along the direction of motion of the symmetry point is a small fraction of T. The tension T due to the purse strings is many times larger than the force due to either the amnioserosa, by a factor of 2–5, or the bulk of the lateral epidermis, by a factor of 6–15 (second ladder). Moreover, all the applied stresses are at least two orders of magnitude larger than the drag (first ladder).

In *Drosophila*, nonmuscle myosin II (herein called *zip*/MyoII) is a hetero-hexamer comprised of a pair of heavy chains, a pair of essential light chains, and a pair of regulatory light chains. Each subunit is encoded by a single gene,

and the heavy chains, which make this myosin unique, are encoded by the *zipper* gene (Kiehart *et al.*, 1989; Karess *et al.*, 1991; Young *et al.*, 1993; Edwards *et al.*, 1995). *zip*/MyoII is the molecular motor that drives shortening of the actomyosin purse strings and the contractile apparatus of the amnioserosa (Franke *et al.*, 2005). Both immunofluorescent strategies and localization of GFP-tagged *zip*/MyoII (GFP-*zip*/MyoII) demonstrate that *zip*/MyoII is localized to the purse string in a "bars on a string" pattern. GFP-*zip*/MyoII is functional—it can rescue the embryonic lethal phenotypes of embryos that lack zygotically encoded *zip*/MyoII. Moreover, analysis of "transgenic mosaics" demonstrates that this myosin drives active contractility. We surmise that during closure active contractility is mediated by the *zip*/MyoII motor protein acting on an actin substrate and fueled by the hydrolysis of ATP. Nevertheless, we cannot rule out that some tension in each tissue is due, at least in part, to additional elastic (i.e., passive) behavior of the stretched elements in the purse string, in cell junctions or in other parts of the cell or extracellular matrix.

Signaling downstream of small GTPases in the Rho subfamily activates nonmuscle myosin II contractility by modulating both the extent of myosin regulatory light chain phosphorylation (by both stimulating kinase function and inhibiting phosphatase function) and the assembly of actin into appropriate filament networks or bundles (Bresnick, 1999; Lu and Settleman, 1999; Ridley, 2006; Lee *et al.*, 2007). RhoA protein is loaded maternally to contribute to early movements in *Drosophila* embryogenesis (e.g., cellularization, Crawford *et al.*, 1998) and at least some of the maternal load of RhoA protein perdures (i.e., remains present) until dorsal closure (Wood *et al.*, 2002). *RhoA* also interacts genetically with nonmuscle myosin II in *Drosophila* (Halsell and Kiehart, 1998; Halsell *et al.*, 2000; Winter *et al.*, 2001). *RhoA* (Magie *et al.*, 1999; Bloor and Kiehart, 2002), *Rac* (Harden *et al.*, 1995; Hakeda-Suzuki *et al.*, 2002), and *Cdc42* (Genova *et al.*, 2000) all contribute to closure as well as other cell movements. Bloor and Kiehart (2002) showed that ectopic expression of $RhoA^{N19}$, which behaves as a dominant negative, disrupts purse string formation and therefore its function.

Wound healing in response to mechanical perturbation and/or laser ablation of closure stage embryos has been studied previously (Kiehart *et al.*, 2000). When lesions were made across the purse string, an actin rich, supracellular purse string formed within minutes of wounding. This secondary purse string extended around the lesion in both the lateral epidermis and the amnioserosa. With time it appeared to contract, thereby stretching the cells to close the wound. These observations were confirmed and extended to show that myosin was also recruited to the wound edge (Wood *et al.*, 2002). These studies also showed that the free edges of wounds formed in *RhoA* null mutant embryos failed to assemble a continuous actin cable. Such wounds closed after considerable delay, through alternative mechanisms that entailed the extension of lamellipodia and filopodia. Depending on the shape of the lesion, closure also involved zipping of cells at the wound margin. Interestingly, when cells expressed dominant negative *Cdc42*, a RhoA dependent purse string could constrict but failed to close a tiny hole that remained following constriction. In contrast, triple mutants that knock–out all Rac function in the embryo had no effect on wound closure. RhoA protein contributes to the wound response of vertebrate cells in culture, of chick embryo epidermis, and of frog oocytes. In each case, RhoA is required for formation of a contractile purse string (Martin and Lewis, 1992; Mandato and Bement, 2001; Bloor and Kiehart, 2002; Martin and Wood, 2002).

These observations on *zip*/MyoII function and regulation provide evidence for actomyosin-based mechanisms for both purse string and amnioserosa contractility. Nevertheless, we do not have an adequate understanding of the contractile assemblies that constitute the purse strings in the leading edge nor the cortical arrays in the amnioserosa. Neither do we know which cytoskeletal accessory proteins participate in the structure and function of the distinct actomyosin assemblies that characterize these tissues.

Here we investigate the function, regulation, and structure of the purse strings. We analyze the contribution of the purse string to closure by removing some or all of a leading edge of the lateral epidermis and its component purse string through laser microsurgery, then characterize a five phase response to purse string removal. Key features of the response to surgery include: inhibition of closure while the free edge of the lateral epidermis formed by the laser incision recoils away from the dorsal midline; formation of new, secondary contractile purse strings; and subsequent resumption of closure. Zipping between cells with native and secondary purse strings can occur provided sufficient time passes between the formation of the laser lesion and incorporation of the secondary purse string into the canthi. Uncut regions of the purse string retain their native morphology except at regions immediately adjacent to the site of incision. We also show that α-actinin, an actin cross-linking/bundling protein, is an integral part of native purse strings, where it accumulates as a cytoplasmic component of cell junctional complexes in a punctate pattern that alternates along the length of the supracellular purse strings with the more centrally localized nonmuscle myosin II. Moreover, α-actinin is not observed in the amnioserosa. Thus, this accessory protein distinguishes the contractile structures that characterize these two contributing tissues.

RESULTS

A five phase response characterizes the surgical removal of the contractile cable

To investigate purse string function in dorsal closure, we surgically remove ~1/2 of the cells of one leading edge with a

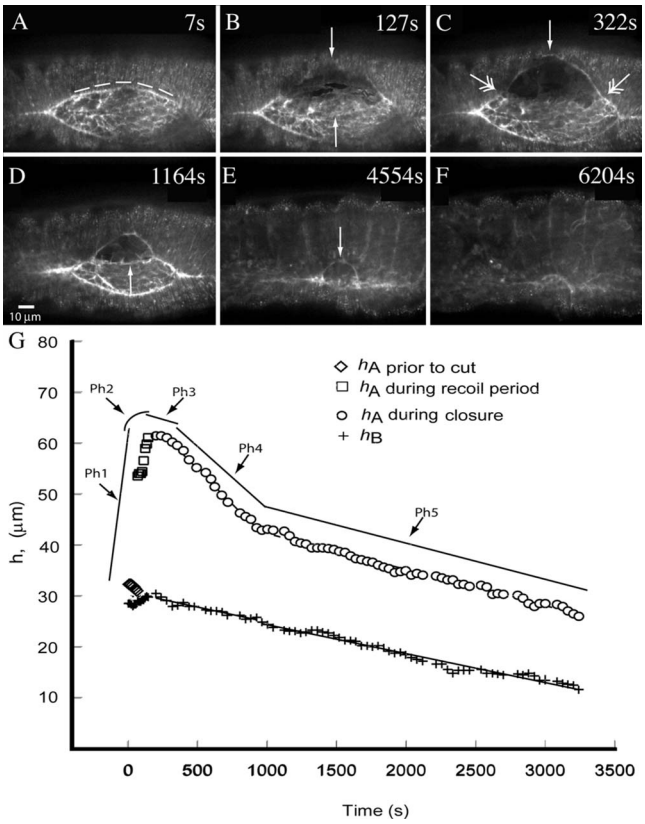

Figure 2. Confocal micrographs show formation of a new, secondary purse string in response to surgical removal of a large fraction of leading edge cells and their contractile, native purse string. Fluorescence in all panels is from GFP-moe, which binds to F-actin. An embryo in mid-closure is shown in A (area of the exposed amnioserosa is ~4000 μm^2). The trajectory of the laser surgical cut is shown by the dashed line. Upper and lower arrows in B indicate the free edge of the remaining lateral epidermis and amnioserosa, respectively ~2 min after the laser surgery. Between B and C, a secondary purse string begins to form (arrow in C). The junction between the native purse string and the secondary purse string is depicted by double arrows. The arrow in D points to a secondary purse string formed in the amnioserosa. In E, closure is nearly complete and the arrow points to the secondary purse string in the lateral epidermis. In F, closure is complete. Scale bar in D is for panels A–F and is 10 μm. Panel G plots h_A (ipsilateral to the cut) and h_B (contralateral to the cut) prior to and after laser surgery. The surgically produced free edge (open squares), the newly formed secondary purse string (open squares and circles), the position of the purse string in the uncut lower leading edge (crosses), are plotted as a function of time. Lines are hand drawn as guides and depict the five phases of the response to the spaceship cut protocol, Ph1–Ph5.

steered UV microbeam (Fig. 2; Supplemental Video 2). During surgery, we observe cell and embryo morphology using time-lapsed, spinning disk confocal microscopy of GFP-moe fluorescence, which allows us to visualize F-actin (Kiehart *et al.*, 2000). We steered the microbeam in an arc that extends from anterior to posterior (or visa versa), starting ~1/4 of the way from one canthus to approximately ~1/4 of the way to the other canthus [see dashed trace in Fig. 2(A), before cut, double arrows in Fig. 2(C), after cut]. The incision ablates the cells of the leading edge, the contractile cable that they include and the row of amnioserosa cells that lies below them [Fig. 2(B)]. A total of ~20 embryos were interrogated by this procedure, of which three were used for statistical analysis and measurements (see Experimental Procedures). Laser surgery leaves "free edges" of lateral epidermal and amnioserosa cells [arrows in Fig. 2(B)] that define new margins for both tissues and causes a reproducible response characterized by five phases, which relate changes in F-actin localization and in *h* (the maximal distance between the new leading edge and the dorsal midline) to time [Fig. 2(G)]. These phases are as follows:

Phase 1: Recoil. The cut margin of the lateral epidermis [upper arrow in Fig. 2(B) and arrow between two double arrows in Fig. 2(C)] recoils away from the dorsal midline at a rate of 916.4±156.8 nm/s (n=3) and has a smaller radius of curvature than the arc of the original purse string. Concurrently, the cut margin of the remaining amnioserosa tissue [lower arrow in Fig. 2(B)] retracts towards the dorsal midline.

Phase 2: Secondary purse string formation. Towards the end of recoil and overlapping with the turning point in phase 3, new purse strings rapidly assemble at the margins of the intact cells in the retracting "free edges" [Ph2 in Fig. 2(G), upper arrows Fig. 2(B)]. These secondary purse strings form in cells that are distinct from those destroyed by the microbeam—i.e., cells that assemble a secondary purse string *did not* contain a purse string during native closure. Because of the overall morphology of the embryo when it resumes closure, we refer to the laser surgeries that generate this morphology as spaceship cuts, e.g., Fig. 2(D).

Phase 3: The turning point and plateau. With time, the secondary purse string matures and ultimately recoil stops at a turning point [*h* plateaus, Fig. 2(C), Ph 3 in Fig 2(G)]. The plateau lasts several minutes (6.5±1.4 min, n=3). In 2 of 7 embryos, a ~straight edge, parallel to the dorsal midline, forms in the amnioserosa, indicating a taught secondary purse string [arrow in Fig. 2(D)]. In other embryos, this edge was more ragged.

Phase 4: Resumption of closure at a fast, super-native rate and Phase 5, completion of closure at a native rate. Once the secondary purse string matures, closure resumes with an initial, "super-native" rate [28.3±5.4 nm/s, n=3, Ph4 in Fig. 2(G)] that subsequently settles to rates indistinguishable from native [7.2±2.4 nm/s, n=3, Ph5 in Fig. 2(G)]. Note, these rates are indistinguishable from that of native closure in both our uncut control embryos (6.0±0.8 nm/s, n=5) and our previously published, native embryos (Hutson *et al.*, 2003; Homsy *et al.*, 2006; Peralta *et al.*, 2007). Following spaceship cuts, closure of the interrogated side of the embryo is delayed relative to the uncut side (43.3±10.9 min, n=3).

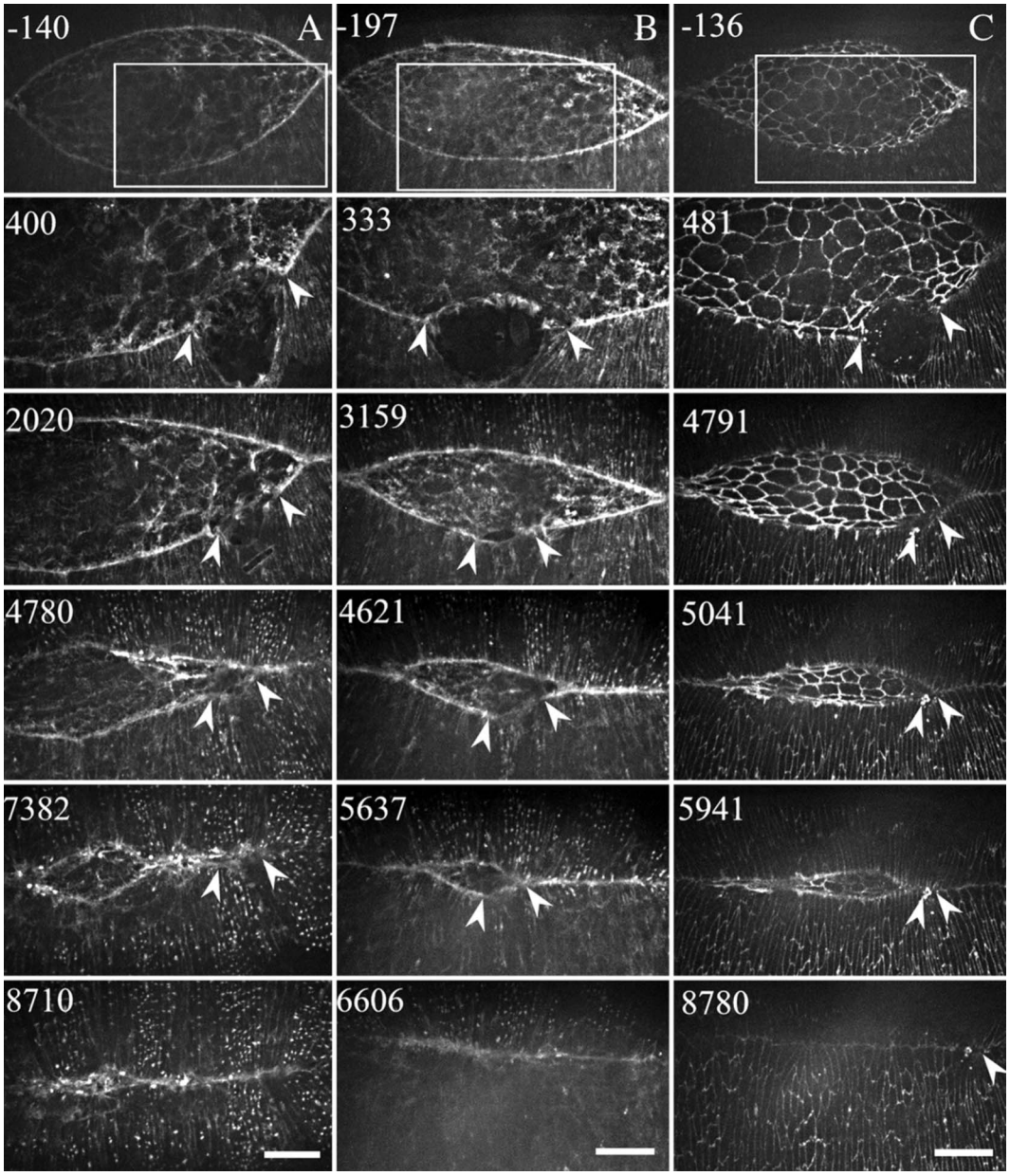

Figure 3. Columns of confocal images show zipping and closure in three spaceship cut embryos expressing GFP-moe (A and B) or GFP–*D*E–cadherin (C). In this figure, time zero is the time of the cut and times are shown in seconds for each image in the column. The first image in each column shows the region of interest, which is tracked in time at high magnification following surgery. Pairs of arrowheads show the margins of the surgical cuts. Single arrowheads in the last row of images indicate an embryo in which a small aggregate of debris was swept into the seam of the closed embryo (column C). Scale bars (20 μm) in the last row of images only apply to the high magnification micrographs.

Secondary purse strings can participate in zipping

The ability of leading edge cells that included a secondary purse string to zip into an approaching canthus as dorsal closure proceeds was investigated in both F-actin labeled (GFP-moe) and GFP-*D*E–cadherin labeled embryos which localizes to adherens junctions (Oda and Tsukita, 2001). We find that the progress of zipping between leading edges containing secondary and native purse strings depends on when during closure the spaceship cut was performed [$n=7$, Fig. 3, Supplemental Videos 3(A)–3(C)—it is particularly important to view the GFP-moe Videos 3(A), 3(B), and the GFP–*DE*–cadherin, Video 3(C) to assess the data]. When cuts were made early in closure, the secondary purse string had time to catch up to flanking segments of the native purse string (i.e., the native and secondary purse strings fell on one continuous arc). When this occurred before the secondary purse string entered the canthus, zipping proceeded normally or almost completely normally and on time [Figs. 3(B), 3(C)

Supplemental Videos 3(B), 3(C)]. In contrast, when the secondary purse strings were not fully recovered (i.e., a sharp angle remained between the native and secondary purse strings as the boundary was about to enter the canthus), zipping was slowed or transiently inhibited [Fig. 3(A), Supplemental Video 3(A)]. In such embryos, all apposing native purse strings completed closure, then contractility in the secondary purse string mediated the remainder of closure. We surmise that zipping is quite normal when the geometry of the two zipping edges matches well, but zipping is perturbed if there is discrepancy in the width of the zipping cells or the angle that the zipping leading edges make with the dorsal midline. In the case of discrepancy, zipping eventually occurs, but abnormally. For example, it did so in fits and starts, often skipping over regions that included secondary purse string, only to have zipping proceed from an internal seam, as we observed with the double canthus nick experiments (Hutson *et al.*, 2003; Peralta *et al.*, 2007). Alternatively, complete seam formation between secondary and native leading edges occurred "edge to edge," as we often observe for the very end stages of closure.

Laser incisions only perturb tissue morphology locally

After spaceship cuts, remaining stretches of native purse strings experience a transient delay in closure, then proceed almost completely on schedule. On both the cut, ipsilateral side [side A, Fig. 2(C), between the double arrows and the canthi], and on the opposite, contralateral side (side B), undamaged purse strings and leading edges undergo a small and transient recoil that is followed by closure at native rates [Figs. 2(B)–2(F)]. Only regions that are directly adjacent to the ablated tissue are more grossly affected—they retract away from both the dorsal midline and the laser lesion [regions near double arrows in Fig. 2(C)] while the remainder of the tissue maintains its overall morphology. Subtle movements in these regions can be observed by quickly flipping back and forth between frames taken just before and just after the cut (Supplemental Video 2). Together, the data confirm that the bulk of tension released following laser incisions occurs *locally*. Thus, locally anchored contractile and/or elastic elements can drive morphogenesis in unperturbed regions even when adjacent regions lack a purse string or normal attachments to other tissues.

Myosin II accumulates in a "bars on a string" pattern in secondary purse strings

To investigate *zip*/MyoII in secondary purse strings, we make spaceship cuts in embryos that ubiquitously express GFP-*zip*/MyoII heavy chain. We found that GFP-*zip*/MyoII accumulates in a bars on a string pattern in the secondary purse string just as in native purse strings [compare region between arrows in Fig. 4(A) and Fig. 4(B), Supplemental Video 4].

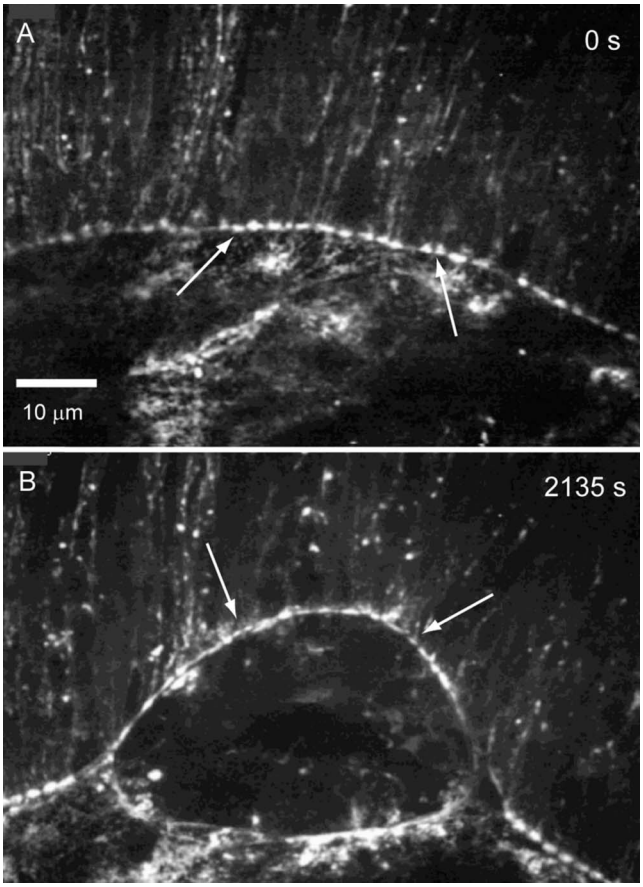

Figure 4. Confocal micrographs show nonmuscle myosin II in native and secondary purse strings. High resolution images of the interface between the lateral epidermis and the amnioserosa in an embryo expressing GFP-*zip*/MyoII heavy chain is shown before (A) and after (B) a spaceship cut. The "bars on a string" pattern is apparent in both native and secondary purse strings. Arrows in A and B depict regions with particularly conspicuous bars on a string pattern. Scale bar in A is for both panels and is 10 μm.

Secondary purse strings are contractile, robust and resilient

Next we investigate secondary purse string contractility with laser microsurgery, show that secondary purse strings are under tension and are robust, such that tertiary purse strings form in response to their removal. We first repeat the spaceship experiment to make a secondary purse string [Figs. 5(A)–5(D), see Supplemental Video 5], then nick the secondary purse string [arrow in Fig. 5(D)]. Each of the four embryos responded to surgery in a qualitatively similar fashion (not all phases could be assessed by active contours nor quantitatively analyzed). Prior to surgery, the embryo closes at a native rate of 7.1 ± 0.9 nm/s [$n=4$, PhN, Fig. 5(I)]. Following the first spaceship cut, the tissues recoil (Phase 1 at 963.6 ± 298.0 nm/s, $n=4$) and a secondary purse string forms (Phase 2), recoil stops at a turning point and is followed by a plateau in h versus t (Phase 3). Closure resumes at a super-native rate (Phase 4 at 41.3 ± 2.5 nm/s,

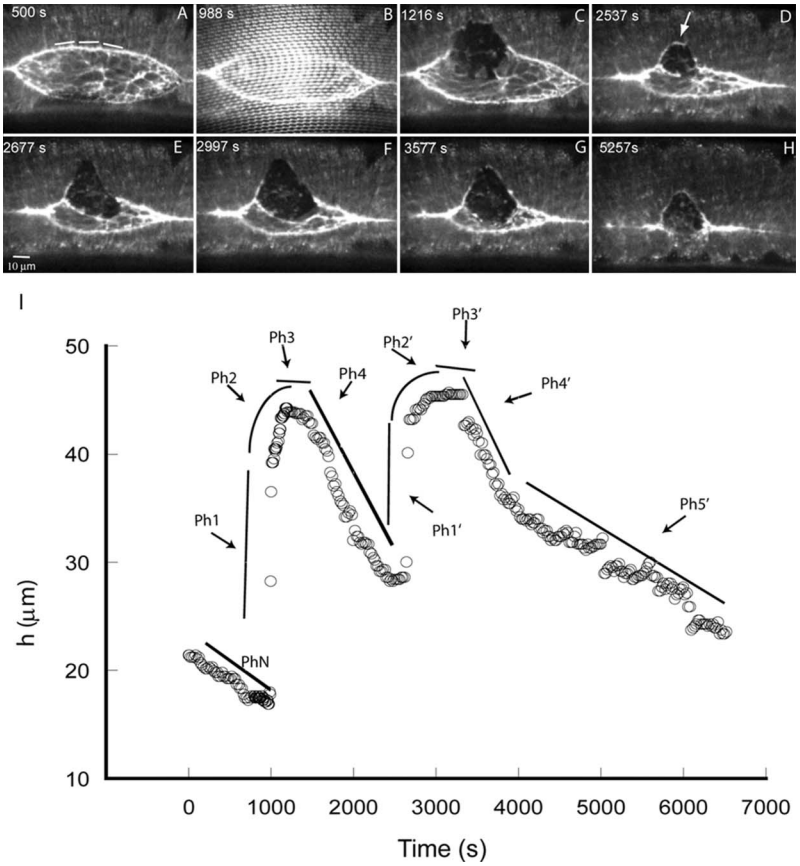

Figure 5. Confocal micrographs show that the secondary purse string is under tension and when cut, forms a tertiary purse string. (A–H) Time-lapsed confocal analysis of a GFP–moe expressing embryo subjected to two laser surgical protocols. Panel A shows an embryo prior to a spaceship cut where the dashed line indicates the position and extent of the cut. Panel B was taken during a cut and shows the autofluorescent bloom due to endogenous fluorochromes in the embryo (see Experimental Procedures). C and D show recovery from surgery. Arrow in D shows the targeting of a second cut. Panel E shows recoil from the second cut. Panels E through H show recovery following the second cut where closure eventually completed successfully (not shown). Panel I graphs *h* as a function of time (see text). Lines are drawn as guides to the eye and phases (Ph) are described in the text.

$n=2$). At this point, we nick the secondary purse string [Fig. 5(D), arrow], observe rapid recoil (428.5±112.3 nm/s, $n=3$, Phase 1′) then observe the formation of a "new secondary" (in this case, "tertiary") purse string (Phase 2′) that goes through a characteristic turning point and plateau (Phase 3′). The tertiary purse string recovers at a fast, super-native rate (Phase 4′, 29.4±3.0 nm/s, $n=2$), then completes closure at nearly native rates (Phase 5′, 5.4±0.7 nm/s, $n=4$). Thus, the response to surgery is comparable whether native or secondary purse strings are contributing to closure.

Recoil dynamics following laser surgery reveal fundamental differences in tissue mechanics

To further investigate the mechanical properties of the native purse string and the tissues that include and surround it, we "nick" the leading edge with the microbeam, then track fiducial points in adjacent cells in the embryo (Fig. 6, see Supplemental Video 6). This laser surgery allows us to evaluate how tension is released in different cells that contribute to closure. Each cut ablates several leading edge cells and their purse string as well as the amnioserosa cells that lie below them. For these experiments, we dramatically improved contrast of cell boundaries by using embryos that carry the GFP–*D*E–cadherin transgene, which labels adherens junctions, but lose our ability to image the actin rich purse string directly. In Fig. 6(A), the green bar specifies the target of the laser incision and the colored dots identify the fiducial points at the time just before the incision in cells of the leading edge (red), the lateral epidermis (blue), and the amnioserosa (yellow). Note that two amnioserosa cells (asterisks) were destroyed in the embryo shown, the one targeted by the laser and one adjacent to it on the right. In Fig. 6(B), colored tracks record the history of motion for the 15 s following the laser incision (i.e., until rapid changes in tissue morphology ceased). The colored dots locate the position of the fiducial points at 15 s.

The boxed fiducial points in Figs. 6(A) and 6(B) draw attention to the recoils of a cell for each of the tissues. The red points are 8.9% closer and the blue points are 26% closer [Fig. 6(B) versus Fig. 6(A)]. Thus both the leading edge cell and the lateral epidermal cells shortened in response to the cut. In contrast, the recoil of an amnioserosa cell is more complex. Tracking four boxed yellow fiducials in Fig. 6(A), Fig. 6(B) reveals that the edge closest to the laser incision *lengthens* by 41%. Going clockwise, the other three edges *shorten* by 30%, *lengthen* by 3.2%, and *shorten* by 25%. This indicates a complex gradient in the stress fields experienced by a single amnioserosa cell following the laser incision.

To estimate the size of the region of released tension due to this laser nick, we plot fractional changes in the width along the length of the leading edge (fiducial points corre-

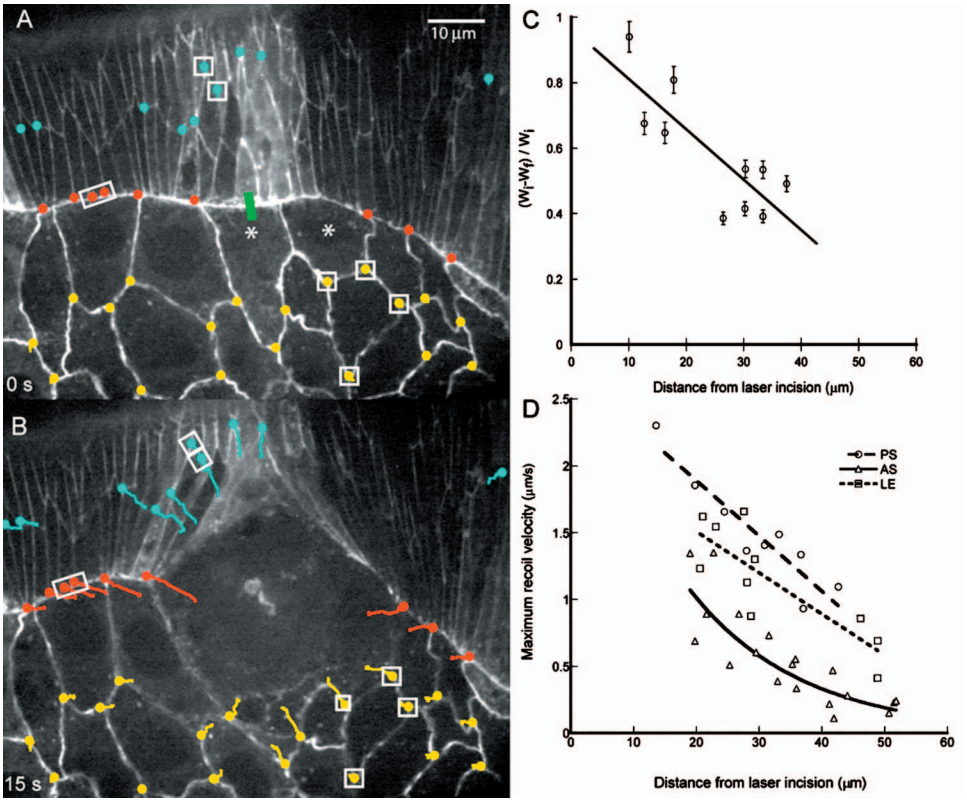

Figure 6. Fluorescent micrographs of cell junctions document initial tissue response to laser cuts. (A–B) Time-lapse confocal micrographs of a GFP-*D*E-cadherin embryo show adherens junctions in a small region of amnioserosa juxtaposed to leading edge, before (A) and after (B) laser surgery. Time is arbitrarily set to zero in A and the 10 μm scale bar in A is for both panels. The green bar in Panel A shows the site of laser nicking. (B) The same region after the leading edge was nicked with a short linear cut (~3 μm long) that ablates ~4 leading edge cells. Fiducial points along the supracellular purse string (red), in the lateral epidermis (blue) and the amnioserosa (yellow) are shown prior to nicking in panel A, their tracks with time after nicking and their resting point after the end of recoil are shown in panel B. Panel C plots the normalized width of a leading edge cell $(W_i - W_f)/W_i$, as a function of the distance from the site of the laser lesion where W_i and W_f are the initial (before the cut) and final (at the end of recoil) widths of individual leading edge cells. The least squares fit of the data show that beyond 60 μm no change in width is expected to occur. Panel D plots the maximum recoil velocity of the fiducial points versus distance from the site of the laser incision and fit lines also extrapolate to ~60 μm.

spond to cell boundaries) and the maximum recoil velocity for all the fiducials, each as a function of distance from the center of the laser lesion [Figs. 6(C) and 6(D)]. Adjacent to the nick, remaining sections of native purse string shorten in response to surgery [Fig. 6(C)]. Extrapolating the fitted curves for each of these three data sets also suggests that tension is released outwards from the center of the nick to ~60 μm. Similarly, in Fig. 6(D) for each of the three tissues we observe the highest maximum velocities closest to the laser lesion with the recoil rate decreasing as a function of distance. Note that while the data for the purse string and lateral epidermis exhibit essentially linear falloff, the amnioserosa data fall off quadratically [Fig. 6(D)]. This is not surprising given that recoil is both along the long axis of the columnar cells in the lateral epidermis and along the short axis of the same cells and therefore along the axis of the purse string. In contrast, recoil in the amnioserosa involves complex two-dimensional remodeling of the polygonal cell meshwork that characterizes the tissue [Fig. 6(B)]. It follows that: nicking releases tension in the tissues that may be due to active (contractile) and/or passive (elastic) processes produced or stored in the cytoskeleton and extracellular matrix of these tissues and that each tissue has unique mechanical properties (see Franke *et al.*, 2005).

The purse string is contractile in the absence of attached amnioserosa

To determine whether or not contractility of the amnioserosa might contribute to super-native rates observed during recovery, we perform two sequential surgical cuts (Fig. 7, Supplemental Video 7). First, we cut the amnioserosa away from the leading edge with an arc just dorsal of the leading edge cells, using a surgical edge cut [$n=6$, see dashed line in Fig. 7(A), for edge cuts, see Peralta *et al.*, 2007]. This cut may leave intact some or all of the amnioserosa cells that are tucked under the leading edge of the lateral epidermis. Following edge cuts, the lateral epidermis recoils away from the dorsal midline, reaches a turning point and plateau, then resumes

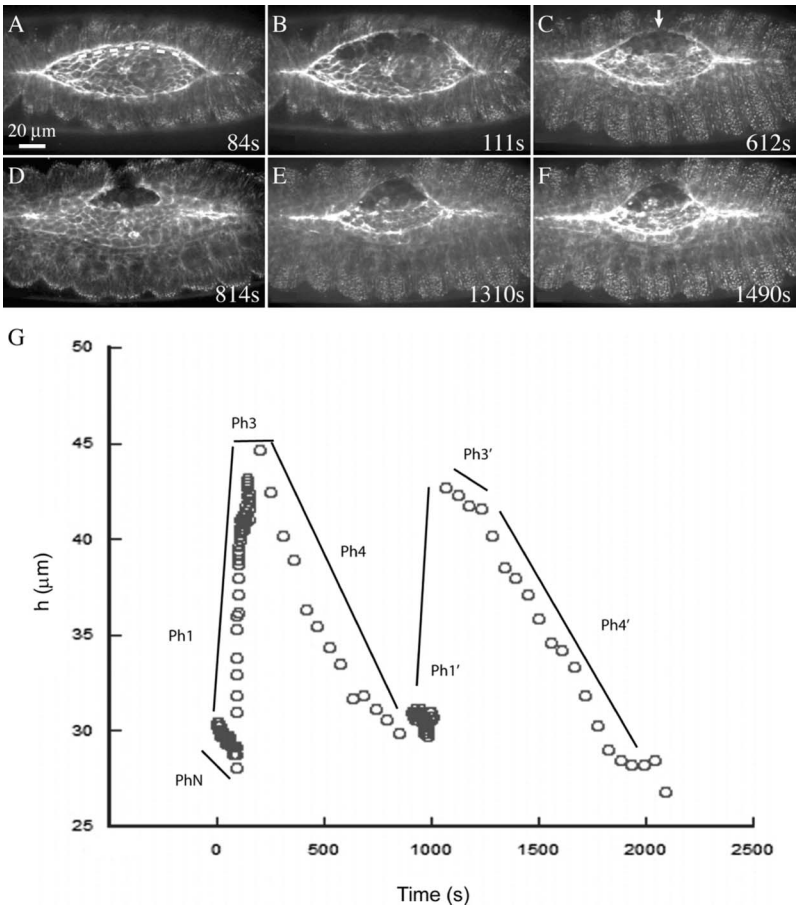

Figure 7. Purse string tension is independent of the amnioserosa. Time-lapsed confocal micrographs of a GFP-moe expressing embryo during dorsal closure. Scale bar in A applies to panels A–F. An embryo (A) just before (~1 s) initiation of an edge-cut protocol, where the dashed line indicates the targeted path of the laser during surgery. Following the edge cut, tissue recoils through the turning point (B), then closure resumes (C). The edge cut embryo seconds after the detached purse string was nicked with a second laser cut (D). A secondary purse string forms (E) and closure resumes (F). A plot of *h* versus time (Panel G, see text), where hand drawn lines are guides to the eye. Note that there is no Ph2 because a secondary purse string does not form after an edge cut—the native purse string is stretched until forces balance and the turning point is reached.

closure [Fig. 7(C)]. Once closure resumes, we cut the purse string with a short linear cut across the purse string [arrow in Fig. 7(C) shows site of future cut]. A multiphase response ensues [Fig. 7(G), Ph1′–Ph4′]. The laser disrupts the purse string, creating two free ends that recoil away from one another, showing that the cable is contractile even when it is not attached to the bulk of the amnioserosa [Fig. 7(D)]. The new free edge formed by unablated lateral epidermal cells also recoils away from the dorsal midline (Phase 1′). A secondary purse string begins to assemble, matures, reaches a turning point, and plateaus (Phase 3′, see also Fig. 10 in Kiehart *et al.*, 2000). Both the amnioserosa-independent leading edge and the secondary purse string resume closure at an initial, super-native rate (30.1±2.3 nm/s, Phase 4′), then closure slows (6.1±1.4 nm/s, $n=5$, indistinguishable from native rates). This multistep experiment establishes that purse strings isolated from amnioserosa are contractile.

RhoA is required for assembly and shortening of secondary purse strings

To evaluate regulation of secondary purse string assembly, we cut *RhoA* mutant embryos with spaceship [$n=4$, Figs. 8(A)–8(D), Supplemental Video 8(A)] and line [$n=5$, Figs. 8(E)–8(H), Supplemental Video 8(B)] cuts. In these embryos, the native purse string is not as robust as in wild-type embryos, so we increase both exposure time and contrast to obtain a reasonable image. In addition, closure proceeds slowly in native, *RhoA* mutant embryos ($dh/dt = 3.2\pm1.1$ nm/s, $n=5$). Following spaceship cuts in these embryos [dashed line in Fig. 8(A) indicates the trajectory of the cut], little or no GFP-moe fluorescence accumulates at the margin of the cut [compare Figs. 8(B)–8(D) to Figs. 2(B)–2(F)], indicating that RhoA function is required for complete secondary purse string formation. With time, fragments of weak secondary purse strings [double arrows in Fig. 8(C)] form along the free edge. Other regions lack purse strings altogether [arrows in Fig. 8(C)], even long after secondary purse strings in wild-type controls assemble, contract, and effect closure [compare time course in Figs. 8(B)–8(D) versus Figs. 2(B)–2(F)].

The weak native purse strings seen in *RhoA* mutant embryos before laser surgery and the weak secondary purse strings after surgery are most likely due to the perdurance of residual RhoA protein that remains from the maternal load of this protein or its message in these embryos. This interpretation is supported by the observation that appropriately expressed dominant negative *RhoA* perturbs closure by disrupting purse string and amnioserosa function early (Magie *et al.*, 1999; Bloor and Kiehart, 2002). Following spaceship

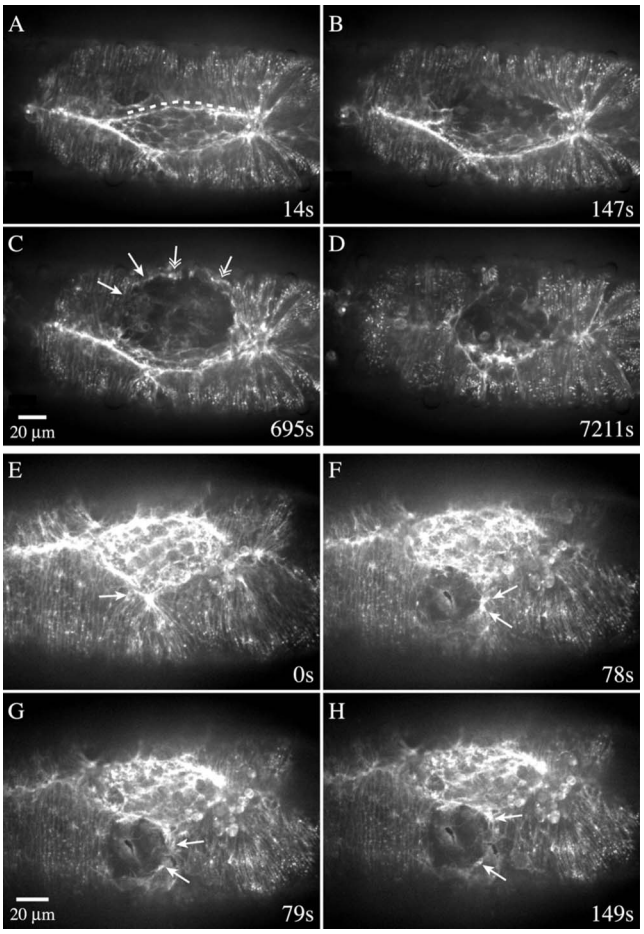

Figure 8. Recovery from laser surgery is inhibited or delayed in zygotic, *RhoA*$^{E3.10}$ loss of function homozygotes. Time-lapsed confocal micrographs of GFP-moe embryos homozygous for *RhoA*$^{E3.10}$. The first embryo was subjected to a spaceship cut (A–D). A second embryo was laser nicked with a shorter cut (E–H). The 20 μm scale bar in C is for A–D and in G is for E–H. *RhoA*$^{E3.10}$ mutant embryos fail to form secondary purse strings following a spaceship cut (B–D). Some F-actin accumulates (arrows and double arrows in C), but an intact, secondary purse string never forms. After a brief period of recovery, dorsal closure fails (D). In contrast, a secondary purse string forms in *RhoA*$^{E3.10}$ embryos subjected to a smaller laser cut (arrow in E). This secondary purse string shows some contractile or elastic behavior (arrows in F–H follow fiducials in the secondary purse string that flank the site of a second laser ablation). Cells retract following tension release, but not as much as in wild-type embryos.

cuts in *RhoA* mutant embryos, dorsal closure always fails, despite the small amount of residual RhoA function [n=4, Fig. 8(D)].

To investigate further laser lesions in *RhoA* embryos, we made small line cuts in the lateral epidermis of additional embryos [arrow in Fig. 8(E)]. When a small surgical lesion is induced in the lateral epidermis in *RhoA* embryos, actin is recruited to the secondary purse string [Figs. 8(F)–8(H)]. The abundance of F-actin as indicated by GFP-moe fluorescence is reduced such that it is comparable to levels of F-actin in the amnioserosa (compare primary and secondary purse strings in *RhoA* mutant embryos, Fig. 8, versus wild-type embryos, Figs. 1 and 2). These observations suggest that RhoA functions during secondary purse string formation in a cell-cooperative fashion—intact cells that surround small lesions and have a low concentration of RhoA can assemble a secondary purse string. In contrast, the intact cells surrounding a large lesion do not form a complete secondary purse string.

We also examined the mechanical properties of the secondary purse strings formed in *RhoA* mutant embryos [Figs. 8(F)–8(H), Supplemental Video 8(B)] by cutting them (with a second laser incision). Such cuts create new free ends that recoil [arrows in Fig. 8(F) versus Figs. 8(G) and 8(H), n=5). However, recoil is considerably slower (22.1±3.2 nm/s, n=5) and not as extensive as in wild-type embryos (47.6±3.2 nm/s, n=7). These data show that secondary purse strings in *RhoA* mutant embryos are not as contractile and/or elastic as those in wild-type embryos.

Secondary purse strings rescue closure following complete removal of native purse strings

To explore further the contribution of secondary purse strings to closure, we targeted *both* leading edges with the microbeam in order to remove *completely* the native purse strings. (Fig. 9, Supplemental Video 9). Taken just after surgery, Fig. 9(B) shows that with the exception of a small region near the canthus, virtually all of the native purse strings have been removed. With time, secondary purse strings form and closure proceeds. As with less extensive ablations, actin is recruited to the margins of the laser lesion within 3–10 min (n=3). Laser ablation destroys the cells of the leading edge, the row of amnioserosa cells under it and, as a consequence, any visible attachment to the amnioserosa. We see no evidence of attachment that could produce any substantial contribution towards closure from the amnioserosa, nor do we observe the reformation of attachments as closure progresses, as seen with through-focus observations. Each of the three embryos interrogated produce a five phase response that paralleled the five phase response to spaceship cuts. In this case, however, both the initial recovery rate (7.6±1.2 nm/s) and the final rate of closure (3.8±0.6 nm/s) were less than half of what was observed for the spaceship cuts. The ability to form completely new purse strings demonstrate that the mechanisms generating contractile cables at the leading edge are robust and resilient.

Nonmuscle α-actinin localizes to the supracellular purse string and junctional complexes

To understand better the contractile and elastic networks that drive cell shape changes in native purse strings and to evaluate how these networks distinguish themselves from those present in the amnioserosa, we stained fixed, dorsal closure-staged embryos for F-actin (with phalloidin), α-actinin, and

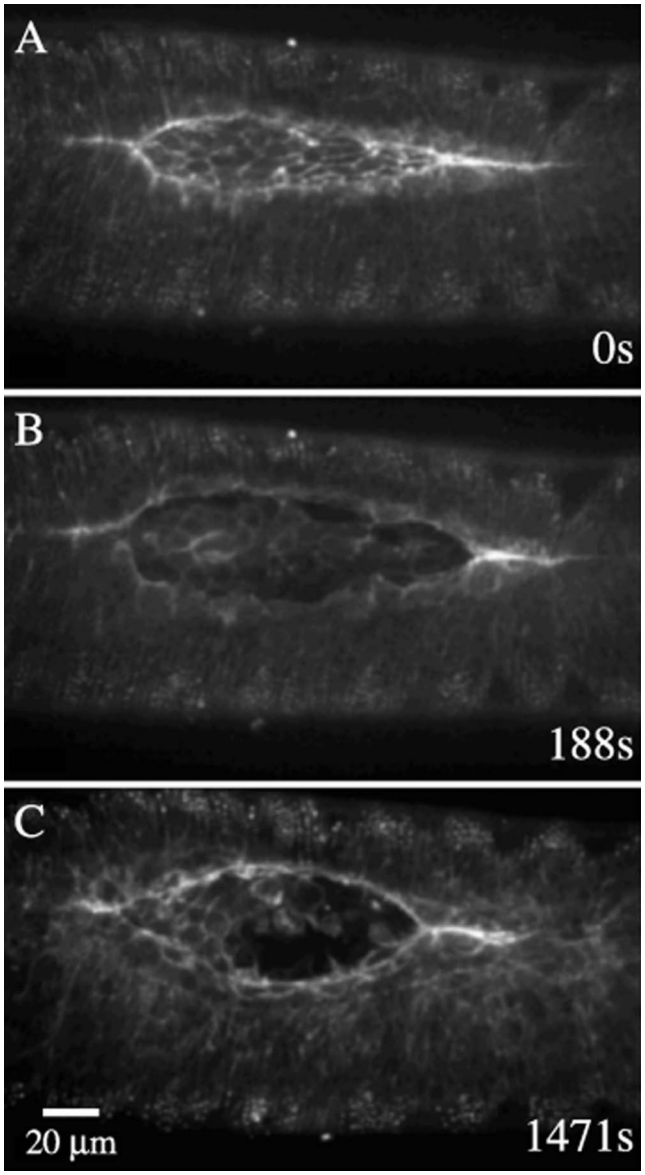

Figure 9. Secondary purse strings form even after the leading edge and the purse strings are nearly completely removed. (A–C) Time-lapsed confocal micrographs of a GFP-moe expressing embryo surgically manipulated late in closure (area of the exposed amnioserosa is ~1350 μm^2). Scale bar in (C) applies to all panels. The embryo in late closure is shown prior to laser surgery (A) and directly following surgery that removed the entire purse string except for a small region near the right hand canthus (B)—note that the leading edges are detached from the amnioserosa. F-actin is recruited to the leading edge (C) to form a secondary purse following which the embryo proceeds to close (the final rate of closure is approximately half the rate of native closure).

zip/MyoII (each with specific antibodies). The α-actinin localizes along the purse string in a punctate fashion, but is essentially absent or is present at substantially reduced levels in the bulk of the lateral epidermis and the amnioserosa [Figs. 10(A)–10(C)]. This contrasts the distribution of F-actin (in fixed embryos or living embryos), which appears essentially continuous along the length of the cable [discontinuities in the cable, which must be present at all cell junctions, are below the limit of resolution of our system, see cables in Fig. 10(B) and Fig. 1(A)]. Embryos triple stained for α-actinin, F-actin, and *zip*/MyoII show that α-actinin puncta are on either side of the cell junctions, while nonmuscle myosin II bars are centered between the puncta of α-actinin [Figs. 10(D)–10(L)], i.e., α-actinin and *zip*/MyoII alternate along the purse string.

We also stained embryos in which the sole contribution of zygotically encoded *zip*/MyoII was tagged with GFP [Figs. 10(D)–10(L), Franke *et al.*, 2005]. The mosaicism of the expression affords a unique opportunity to evaluate the distribution of α-actinin in cells that either express or fail to express zygotic nonmuscle myosin II. In regions that lacked myosin II, actin was present at a reduced level but no puncta of α-actinin were observed [brackets in Figs. 10(D)–10(L)]. This indicates that myosin II is required for recruiting and/or maintaining α-actinin in the purse string.

DISCUSSION

Secondary and tertiary purse strings rescue dorsal closure following laser ablation of some or all of the native purse strings. Surgical ablation of the leading edge cells which include the purse strings causes a reproducible, five phase response to purse string removal that provides insight into the mechanical properties of the tissues that are involved in closure. Key features in the five phase response include the *rapid* assembly of a secondary purse string, its maturation to a contractile purse string that contributes to the characteristic spaceship morphology, and the subsequent resumption of closure to completion. Secondary purse strings form after the removal of the native purse strings even when the bulk of the amnioserosa has previously been removed, suggesting that the amnioserosa is not required for secondary purse string assembly. Moreover, secondary purse strings can zip with native counterparts leading to the formation of a nearly seamless and scar-free epidermal sheet. Laser surgery can be used to remove both leading edges, a process that destroys both native purse string and severs most if not all connections to the amnioserosa. Remarkably, following such extensive surgery, secondary purse strings form within minutes and closure proceeds to completion. Thus the bulk of lateral epidermal sheet movements occur even when most if not all connections between the lateral epidermis and the amnioserosa are severed so that in this case contractility in the amnioserosa does not contribute to closure. We confirm that the RhoA small GTPase contributes to native purse string assembly and that the assembly of a secondary purse string is compromised in zygotes homozygous for severe *RhoA* mutations. Together, these observations point to a key role for the purse strings in dorsal closure—surgical removal of the purse strings causes recoil of the remaining tissues away from their ultimate destination at the dorsal

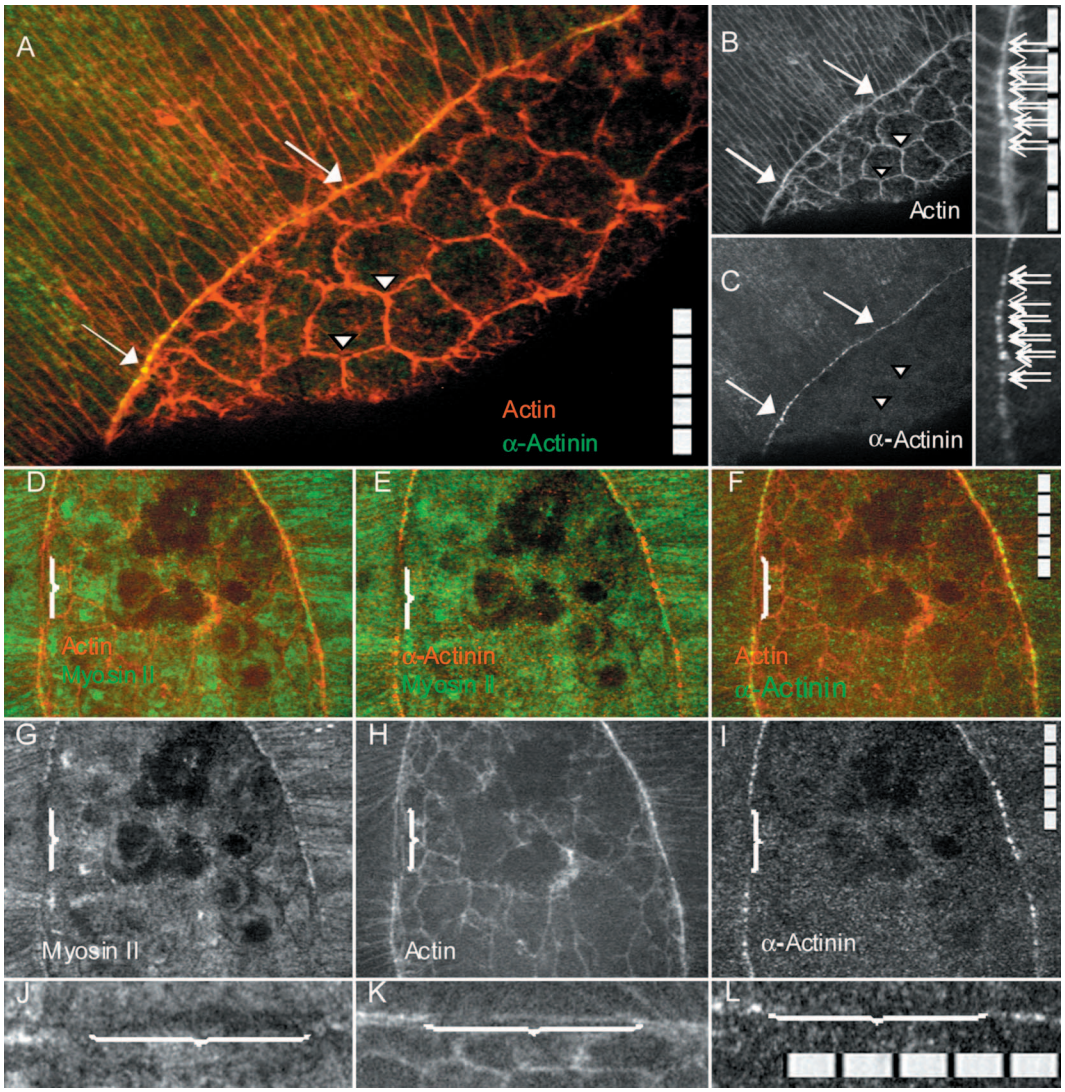

Figure 10. Nonmuscle α-actinin localizes to the purse string but not to the cortical actin meshwork in the amnioserosa. A wild-type embryo double stained for actin and α-actinin (A), overlay of F-actin in red, α-actinin in green; (B) F-actin; and (C) α-actinin. Actin is present in the cortex of the lateral epidermal cells, the amnioserosa cells, and in the supracellular purse string. α-actinin puncta colocalize with a subset of the actin in the purse string (arrows), localize in cell cortices in the remainder of the lateral epidermal cells, and are all but absent in the amnioserosa (arrowheads in C are positioned to coincide with those in A and B). A punctuate pattern of doublets is α-actinin in the purse string at high resolution (arrows in insets B and C) with one spot on either side of the cell junctions. Scale bars in A, the inset in B, F, I, and L are 50 μm in 10 μm increments. (D–L) A segment of leading edge juxtaposed to amnioserosa in an embryo that is a transgenic mosaic for *zip*/MyoII expression and triple stained for F-actin, *zip*/MyoII and α-actinin (see Experimental Procedures for the complete genotype of the embryo and the origin of the mosaic pattern of *zip*/MyoII expression). The region lacking myosin II retains actin but is missing α-actinin (brackets). Pseudocolored merged images with D–F have actin in red and myosin II in green (D); α-actinin in red and myosin II in green (E); and actin in red and α-actinin in green (F). Single channel staining patterns for D–F are for myosin II (G); F-actin (H); and α-actinin (I). An enlarged view of a segment of purse string that includes a region lacking *zip*/MyoII (indicated by brackets, J–L). GFP-*zip*/MyoII is localized in J; F-actin is localized in K and α-actinin is localized in L.

midline and failure of progress towards closure until the embryo generates new contractile cables that can subsequently contribute forces for the resumption of closure.

Unablated cells at the margin of the surgical cut have a "free edge" and can assemble a functional, secondary purse string in a matter of minutes (Bement *et al.*, 1999; Kiehart, 1999; Kiehart *et al.*, 2000; Mandato and Bement, 2001). What induces the formation of a new purse string in cells that never had one before? Studies on mammalian wound healing suggests a number of possibilities that regulate cytoskeletal rearrangements and accompanying changes in cell behavior upon generation of a free edge. These include the cessation of negative cues when neighboring cells are removed (Fagotto and Gumbiner, 1996) and the generation of positive factors that are released from wounded cells (Singer and Clark, 1999; Wood *et al.*, 2002). Several studies

point to the activation of the epidermal growth factor receptor (EGFR) through specific ligands that generate the suite of changes that characterize cells as they respond to the wound. A particularly intriguing study on mammalian cells has shown that the activation of EGFR occurs upon the generation of a free edge in the absence of cell damage (Block *et al.*, 2004). Such activation through EGFR depends on the heparin-binding, epidermal growth factor-like, growth factor (HB-EGF) pathway. The ligand responsible for EGFR activation in free edges is presumably similar to, but distinct from, HB-EGF in itself. The authors conclude that the EGFR is not activated in intact epithelial tissue but sees ligand upon the formation of a free edge. Other changes triggered by the formation of a free edge have been suggested to initiate the wound healing response (see, for example, Song *et al.*, 2004).

What powers the initial resumption of closure at super-native rates? Closure, promoted by secondary or tertiary purse strings formed in response to a variety of different laser interrogation protocols, occurs at two distinct rates. For example, in the spaceship cut protocol (Fig. 2), the secondary purse string and the leading edge drive resumption of closure in two phases. The faster phase (Phase 4) occurs at 28.3 ± 5.4 nm/s. Later, in the slower, Phase 5, closure proceeds at 7.2 ± 2.4 nm/s, which is comparable to native rates (6.0 ± 0.8 nm/s). We envision the supracellular actomyosin purse string (native or secondary) to be assembled from its component parts and anchored locally at cellular junctions. As contraction proceeds due to myosin activity, it is likely that both actin and bipolar myosin filaments become more highly aligned, thereby allowing *zip*/MyoII motors to transmit contractile forces to the junctional complexes more efficiently. As the secondary purse string matures, the concentration of F-actin and *zip*/MyoII in the purse string increases (as assayed by GFP-moe and GFP-*zip*/MyoII fluorescence), suggesting that additional contractile components are being added. However, such a gradual increase in actin and *zip*/MyoII concentration and filament alignment do not correlate with increased rates of closure; instead, closure slows in a notably sharp transition between early super-native rates and final rates that are comparable to native rates. We hypothesize that after initial assembly, the molecular components of the actomyosin purse string work against a low internal load. As the secondary purse string matures, it comes under increased internal load and the rate of closure slows. This change in internal load may be due to strain stiffening as has been observed in purified solutions of actin, actin plus cross-linkers and actin plus motors (Gardel *et al.*, 2004; Gardel *et al.*, 2006; Mizuno *et al.*, 2007). By this hypothesis, components of the contractile and junctional apparatus would rearrange themselves in response to mechanical forces that drive closure. We should point out that this model does not readily explain the sharp transition we see between the fast and slower phases of closure. Thus, an explanation for the super-native closure rate remains an open research question.

Laser surgery designed to destroy the purse string in leading edge cells also severs the connection between the lateral epidermis and the amnioserosa. We see no evidence for healing of this connection along any substantial length of the newly formed, leading edge of the lateral epidermis, but cannot rule out that some reconnection of tissues sporadically occurs in small regions along the interface between the two tissues. The shapes of these secondary purse strings are traced by smooth arcs that show striking symmetry around an axis perpendicular to the dorsal midline. Compare the secondary purse strings in Figs. 2 and 5 to the native purse strings studied here (Fig. 1) and previously (Kiehart *et al.*, 2000; Hutson *et al.*, 2003; Peralta *et al.*, 2007). The smooth, convex, and symmetrical shapes of the secondary purse strings in the lateral epidermis indicate that such sporadic connections are not playing a major role in force transmission between the amnioserosa and the new leading edge that includes the secondary purse string. We would expect local connections that transmit substantial forces between tissues to cause the leading edge to kink locally. Indeed, disruption of the mechanical integrity of the entire amnioserosa also gives remarkably smooth and symmetrical leading edge shapes (Hutson *et al.*, 2003; Peralta *et al.*, 2007).

We also have shown that α-actinin is localized adjacent to cell junctions in a pattern that reciprocates with bars of *zip*/MyoII, which are centered between cell junctions. We show that α-actinin's recruitment and/or maintenance in purse strings is *zip*/MyoII dependent, and we show that it is not a prominent component of the contractile cell cortices that characterize the amnioserosa.

Laser surgery has shown that the secondary purse strings are under tension—following laser ablation of a small segment of the secondary purse string, the remaining portions of the purse string recoil away from the site of ablation. Based on structural similarities between the secondary and native purse strings, we speculate that *zip*/MyoII drives contraction of the secondary purse string during closure. Is closure driven by the secondary purse string distinguishable from "wound" closure? The answer is not clear. Under appropriate conditions, zipping between native and secondary leading edge readily occurs and the resulting epithelium is both scarless and seamless. This suggests that cells usually fated to be in the bulk of the lateral epidermis can acquire the ability to zip normally. Under other conditions, i.e., when the secondary leading edge has not fully recovered or "matured" prior to zipping, incorporation into the canthus is delayed considerably. As described in the introduction, zipping can occur to help heal wounds, so it is not clear if normal zipping is indicative of the formation of a "true secondary purse string" versus a wound purse string. However, if co-opting a wound response to complete closure facilitates further development,

it is not clear what the significance of such a distinction might be.

Are the secondary purse strings actively contractile, passively elastic, or a combination of both? Nominally, contractile filament networks can display both elastic and contractile properties (Mooney *et al.*, 1995). Previously we showed that *zip*/MyoII can cause active contraction during closure by monitoring oscillations in the length of adjacent segments of the leading edge in which the levels of myosin varied through the use of a transgenic mosaic strategy (Franke *et al.*, 2005). In the absence of such transgenic mosaic data, it is possible that myosin II contributes a purely passive, elastic role in the function of the secondary purse strings, but we think that this is highly unlikely. A purely passive elastic behavior would require assembly of the purse string and then a prestretch of the assembled purse string to produce tension and force towards closure. Because the secondary purse string assembles during a recoil phase, matures during a plateau phase, and then begins to shorten, this leaves little opportunity for prestretching the bulk of the newly formed purse string. Nevertheless, we cannot rule out that some compliance due to passive elastic properties is in part contributed by actin or myosin filaments themselves (reviewed in Smith *et al.*, 2005) or by entropic properties of the actomyosin purse string (Luan *et al.*, 2008). The prestretching that is required for such passive elasticity might occur as a consequence of active contractility or might be attributable to the mechanical properties of elements of actomyosin-rich purse strings that were assembled before the turning point and full maturation of a functional, secondary purse string.

Purse strings do not reform following large surgical lesions in *RhoA* mutant embryos and dorsal closure fails, thereby providing confirmation of a key role for RhoA in purse string assembly (Wood *et al.*, 2002). RhoA likely contributes to purse string assembly through its effects on both actin and myosin (Glotzer, 2005). RhoA activates actin nucleators in the formin family to stimulate F-actin assembly. It also activates Rho Kinase and inhibits myosin phosphatase in order to increase phosphorylation on serines and threonines that increase myosin filament assembly, actin-activated ATPase activity and result in motility. In *RhoA* mutant embryos, lack of secondary purse strings and failure of embryos to close after spaceship cuts suggests that while mechanisms in the wild-type embryo may compensate for loss of significant portions of the purse strings, these mechanisms are largely absent in the *RhoA* mutant. It is interesting to note that the inability of *RhoA* mutant animals to heal is dependent on the size of the laser lesion we induce—we are currently investigating whether such cooperativity is due to chemical or mechanical consequences of the loss of RhoA function.

Together our experiments address the contribution of the supracellular purse strings to closure. The ability of an embryo that has lost its purse string to assemble one in new leading edge cells that previously had no purse string speaks to the resiliency of closure. The astonishing ability of the purse strings to drive closure, even in the absence of extensive connections between the lateral epidermis and the amnioserosa, establish that morphogenesis of this cell sheet movement depends on redundant cellular systems that can generate forces in the absence of those that typically contribute. We hypothesize that other cell sheet movements, from neural tube closure to epiboly, depend on comparable redundant systems.

EXPERIMENTAL PROCEDURES

Fly stocks

We observe living embryos with four different GFP-fusion, transgenic stocks that were crossed into appropriate wild-type or mutant backgrounds using standard genetic crosses (Roberts, 1998). (1) Otherwise wild-type flies were usually imaged with sGMCA (flies include the genotype w/w or w/Y; $P[sqh::GFP::moe,w^+]$), a construct that fuses GFP to the F-actin binding fragment of *Drosophila* moesin and is expressed ubiquitously by the *sqh* promoter enhancer cassette (Kiehart *et al.*, 2000). For analysis of RhoA, flies of the genotype w^-/w^- or w/Y; $P[sqh::GFP::moe,w^+]$ $RhoA^{E3.10}/SM6$a were crossed *inter se* and progeny of the appropriate genotype were selected based on the brightness of two copies versus one copy of the $sqh::GFP::moe$ transgene on the $RhoA^{E3.10}$ chromosome ($RhoA^{E3.10}$ is characterized in Halsell and Kiehart, 1998; Halsell *et al.*, 2000). (2) For high resolution analysis of cell boundaries at the level of the adherens junctions, we used GFP-*DE*-cadherin driven by the ubiquitin promoter/enhancer cassette (Oda and Tsukita, 2001). (3) GFP-*zip*/MyoII was used to observe the localization of *zip*/MyoII in a background whereby the only *zip*/MyoII expressed zygotically was GFP-*zip*/MyoII (Franke *et al.*, 2005). Appropriate flies were the only fluorescent progeny of a cross between w^-; $P[sqh::Gal4,w^+]$, $sp\ zip^1/SM6$ virgin females and w^-/Y; $P[UAS\text{-}GFP\text{-}zip/MyoII,w^+]$ $sp\ zip^2/SM6$ males. (4) For visualization of the amnioserosa during closure, we used flies expressing UAS-GFP-moe from the UAS-GMA (Bloor and Kiehart, 2002) responder driven in the amnioserosa by the c381-GAL4 (Manseau *et al.*, 1997) driver (appropriate flies were the only fluorescent progeny of a cross between parents that were w^-/w^- or Y; $P[UAS::GFP::moe,w^+]$ and w^-/w^- or w/Y; $P[c381\text{-}GAL4,w^+]$).

Embryo collection and preparation of observation chambers

Flies were maintained using standard methods (Roberts, 1998). Small population cages of the appropriate genotype were used to collect 1–3 h egg lays (usually 50–200 embryos). Embryos were aged 20–22 h at 16–18 °C to yield populations of dorsal closure staged embryos (Kiehart *et al.*,

2000; Kiehart *et al.*, 2006). Using this imaging protocol, wild-type embryos that were not laser interrogated could be imaged for the duration of closure then removed from the chambers. If provided with appropriate food they eclose to adulthood at rates indistinguishable from control embryos that were not mounted in the chamber and imaged.

Collection and analysis of data sets from surgically manipulated embryos

We use laser microsurgery and time-lapsed confocal microscopy to surgically dissect and follow tissue dynamics in *Drosophila* embryos (Kiehart *et al.*, 2006). Image stacks for each embryo were collected and downloaded to ImageJ (http://rsb.info.nih.gov/ij/). Autofluorescence from the embryo [or "bloom" in Fig. 5(B)] was excited by the 355 nm surgical laser and strobed by the spinning disk in our confocal system (the laser emits a 3–5 ns pulse every 100 ms and our exposure time is $\geqslant$500 ms) such that the position of the purse string in some embryos could not always be followed through portions of the experiments. Embryos that could not be followed accurately by active contours or "snakes" (Kass *et al.*, 1987) were not included in statistical analysis. In cases where regions of interest could not be focused in a single optical plane and/or field of view for portion of the experiment, data sets were retained for qualitative analysis, but were excluded from the statistical pool. Parameters were analyzed as a function of time, tabulated, and evaluated using Microsoft Excel (Redmond, WA) and KaleidaGraph software (Reading, PA).

We adjust the energy per pulse and the rate at which the microbeam is steered to deliver a precise energy dose to the embryo. If the energy fluence is below the ablation threshold, photobleaching can occur, but cells are not ablated. If too much laser energy is delivered to the tissue, the embryos are damaged beyond repair as evidenced by "blowout," i.e., yolk and cell debris flow out of the embryo. Such embryos were not included in our analysis and are not reported. When the energy is properly calibrated, embryos respond to various types of cuts in a highly reproducible manner. In each of the experiments described here, at least five embryos were successfully cut and examined unless otherwise noted.

Immunofluorescence

Antibody staining was performed on whole embryos using standard methods adapted for costaining with the actin probe, rhodamine phalloidin. Briefly, embryos were collected as above then fixed in a 1:1 mix of heptane and 8% formaldehyde fix (100 mM Na-Cacodylate, *p*H 7.2; 100 mM Sucrose; 40 mM K-Acetate; 10 mM Na-Acetate; 10 mM EGTA, 8% formaldehyde) for 30 min at room temperature. Embryos were then devitellinized with 85% ethanol before being rinsed in PBT (0.1 M PBS, *p*H 7.4, 0.1% Triton-X 100, 0.1% BSA) and blocked in 25% fetal bovine serum (FBS) for 1 h. Incubation in primary antibody was for 3 h at room temperature or overnight at 4 °C, then embryos were washed in 5% FBS in PBT. Incubations in secondary antibody and phalloidin were for a minimum of 1–3 h at room temperature or overnight at 4 °C. Finally, embryos were washed in 5% FBS in PBT and equilibrated in mounting media (90% glycerol; 0.1% Tris-HCl, pH8.0; 2% propyl gallate).

Antibodies used were as follows: 1:10 dilution of monoclonal rat anti-waterbug α-actinin in 5% FBS (Babraham Bioscience Technologies); 1:1000 dilution of 656 anti-nonmuscle myosin heavy chain polyclonal antiserum (Kiehart and Feghali, 1986); 1:1000 dilutions of FITC, Cy2 or Cy5 labeled secondary antibody (Molecular Probes, Carlsbad, CA). Actin was detected with 1:1000 dilutions (1 μg/ml) of Texas Red phalloidin or Alexa Fluor 568 phalloidin (Molecular Probes).

SUPPORTING INFORMATION

- Supplemental Video 1A.mov
- Supplemental Video 1B.mov
- Supplemental Video 2.mov
- Supplemental Video 3A.mov
- Supplemental Video 3B.mov
- Supplemental Video 3C.mov
- Supplemental Video 4.mov
- Supplemental Video 5.mov
- Supplemental Video 6.mov
- Supplemental Video 7.mov
- Supplemental Video 8A.mov
- Supplemental Video 8B.mov
- Supplemental Video 9.mov

ACKNOWLEDGMENTS

We thank Ruth Montague, Vinay Singh, and Dr. O'Neil Guthrie, Dr. Stephanos Venakides, Dr. Xomalin G. Peralta and Dr. Josef D. Franke for fruitful discussions and advice. This work was supported by NIH GM33830.

REFERENCES

Agnes, F, and Noselli, S (1999). "Dorsal closure in *Drosophila*. A genetic model for wound healing?" *C. R. Acad. Sci. III* **322**, 5–13.

Bement, WM, Mandato, C, and Kirsch, MN (1999). "Wound-induced assembly and closure of anactomyosin purse string in *Xenopus* oocytes." *Curr. Biol.* **9**, 579–587.

Berg, H (1983). Random Walks in Biology, Princeton University Press, Princeton, NJ.

Block, ER, Matela, AR, SundarRaj, N, Iszkula, E R, and Klarlund, JK (2004). "Wounding induces motility in sheets of corneal epithelial cells through loss of spacial constraints." *J. Biol. Chem.* **279**, 24307–24312.

Bloor, JW, and Kiehart, DP (2002). "*Drosophila* RhoA regulates the cytoskeleton and cell-cell adhesion in the developing epidermis." *Development* **129**, 3173–3183.

Bresnick, AR (1999). "Molecular mechanisms of nonmuscle myosin-II regulation." *Curr. Opin. Cell Biol.* **11**, 26–33.

Campos-Ortega, JA, and Hartenstein, V (1985). *The Embryonic Development of Drosophila melanogaster*, Springer-Verlag, New York.

Crawford, JM, Harden, N, Leung, T, Lim, L, and Kiehart, DP (1998). "Cellularization in *Drosophila melanogaster* is disrupted by

the inhibition of rho activity and the activation of Cdc42 function." *Dev. Biol.* **204**, 151–164.
Edwards, KA, Chang, XJ, and Kiehart, DP (1995). "Essential light chain of *Drosophila* nonmuscle myosin II." *J. Muscle Res. Cell Motil.* **16**, 491–498.
See EPAPS Document No. E-HJFOA5-2-003805 for supplemental material. This document can be reached through a direct link in the online article's HTML reference section or via the EPAPS home page (http://www.aip.org/pubservs/epaps.html).
Fagotto, F, and Gumbiner, BM (1996). "Cell contact-depending signalling." *Dev. Biol.* **180**, 445–454.
Foe, VE (1989). "Mitotic domains reveal early commitment of cells in *Drosophila* embryos." *Development* **107**, 1–22.
Franke, JD, Montague, RA, and Kiehart, DP (2005). "Nonmuscle myosin II generates forces that transmit tension and drive contraction in multiple tissues during dorsal closure." *Curr. Biol.* **15**, 2208–2221.
Gardel, ML, Shin, JH, MacKintosh, FC, Mahadevan, L, Matsudaira, P, and Weitz, DA (2004). "Elastic behavior of cross-linked and bundled actin networks." *Science* **304**, 1301–1305.
Gardel, ML, Nakamura, F, Hartwig, J, Crocker, JC, Stossel, TP, and Weitz, DA (2006). "Stress-dependent elasticity of composite actin networks as a model for cell behavior." *Phys. Rev. Lett.* **96**, 088102.
Genova, J, Jong, S, Camp, J, and Fehon, R (2000). "Functional analysis of cdc42 in actin filament assembly, epithelial morphogenesis, and cell signaling during *Drosophila* development." *Dev. Biol.* **221**, 181–194.
Glotzer, M (2005). "The molecular requirements for cytokinesis." *Science* **307**, 1735–1739.
Hakeda-Suzuki, S, Ng, J, Tzu, J, Dietzl, G, Sun, Y, Harms, M, Nardine, T, Luo, L, and Dickson, B (2002). "Rac function and regulation during *Drosophila* development." *Nature (London)* **416**, 438–442.
Halsell, S, Chu, B, and Kiehart, D (2000). "Genetic analysis demonstrates a direct link between rho signaling and nonmuscle myosin function during *Drosophila* morphogenesis." *Genetics* **155**, 1253–1265.
Halsell, S, and Kiehart, D (1998). "Second-site noncomplementation identifies genomic regions required for *Drosophila* nonmuscle function during morphogenesis." *Genetics* **148**, 1845–1863.
Harden, N (2002). "Signaling pathways directing the movement and fusion of epithelial sheets: lessons from dorsal closure in *Drosophila*." *Differentiation* **70**, 181–203.
Harden, N, Loh, HY, Chia, W, and Lim, L (1995). "A dominant inhibitory version of the small GTP-binding protein Rac disrupts cytoskeletal structures and inhibits developmental cell shape changes in *Drosophila*." *Development* **121**, 903–914.
Homsy, JG, Jasper, H, Peralta, XG, Wu, H, Kiehart, DP, and Bohmann, D (2006). "JNK signaling coordinates integrin and actin functions during *Drosophila* embryogenesis." *Dev. Dyn.* **235**, 427–434.
Hutson, MS, Tokutake, Y, Chang, MS, Bloor, J W, Venakides, S, Kiehart, DP, and Edwards, GS (2003). "Forces for morphogenesis investigated with laser microsurgery and quantitative modeling." *Science* **300**, 145–149.
Jacinto, A, Wood, W, Balayo, T, Turmaine, M, Martinez-Arias, A, and Martin, P (2000). "Dynamic actin-based epithelial adhesion and cell matching during *Drosophila* dorsal closure." *Curr. Biol.* **10**, 1420–1426.
Jacinto, A, Wood, W, Woolner, S, Hiley, C, Turner, L, Wilson, C, Martinez-Arias, A, and Martin, P (2002a). "Dynamic analysis of actin cable function during *Drosophila* dorsal closure." *Curr. Biol.* **12**, 1245–1250.
Jacinto, A, Woolner, S, and Martin, P (2002b). "Dynamic analysis of dorsal closure in *Drosophila*: from genetics to cell biology." *Dev. Cell* **3**, 9–19.
Karess, RE, Chang, XJ, Edwards, KA, Kulkarni, S, Aguilera, I, and Kiehart, DP (1991). "The regulatory light chain of nonmuscle myosin is encoded by spaghetti-squash, a gene required for cytokinesis in *Drosophila*." *Cell* **65**, 1177–1189.
Kass, M, Witkin, A, and Terzopoulos, D (1987) "Snakes-active contour models." *Int. J. Comput. Vis.* **1**, 321–331.
Keller, R, Davidson, LA, and Shook, DR (2003). "How we are shaped: the biomechanics of gastrulation." *Differentiation* **71**, 171–205.
Kiehart, D (1999). "Wound healing: the power of the purse string." *Curr. Biol.* **9**, R602–R605.
Kiehart, D, Tokutake, Y, Chang, M-S, Hutson, M, Weimann, J, Peralta, X, Toyama, Y, Wells, A, Rodriguez, A, and Edwards, G (2006). *Ultraviolet Laser Microbeam for Dissection of Drosophila Embryos*, Elsevier Science, Amsterdam.
Kiehart, DP, and Feghali, R (1986). "Cytoplasmic myosin from *Drosophila* melanogaster." *J. Cell Biol.* **103**, 1517–1525.
Kiehart, DP, Galbraith, CG, Edwards, KA, Rickoll, WL, and Montague, RA (2000). "Multiple forces contribute to cell sheet morphogenesis for dorsal closure in *Drosophila*." *J. Cell Biol.* **149**, 471–490.
Kiehart, DP, Lutz, MS, Chan, D, Ketchum, A S, Laymon, R A, Nguyen, B, and Goldstein, LS (1989). "Identification of the gene for fly non-muscle myosin heavy chain: *Drosophila* myosin heavy chains are encoded by a gene Family." *EMBO J.* **8**, 913–922.
Lee, JH, Koh, H, Kim, M, Kim, Y, Lee, SY, Karess, RE, Lee, S-H, Shong, M, Kim, J.-M, Kim, J, and Chung, J (2007). "Energy-dependent regulation of cell structure by AMP-activated protein kinase." *Nature (London)* **447**, 1017–1020.
Lu, Y, and Settleman, J (1999). "The role of rho family GTPases in development: lessons from *Drosophila* melanogaster." *Mol. Cell. Biol. Res. Commun.* **1**, 87–94.
Luan, Y, Lieleg, O, Wagner, B, and Bausch, AR (2008). "Micro- and macrorheological properties of isotropically cross-linked actin networks." *Biophys. J.* **94**, 688–693.
Magie, CR, Meyer, MR, Gorsuch, MS, and Parkhurst, SM (1999). "Mutations in the Rho1 small GTPase disrupt morphogenesis and segmentation during early *Drosophila* development." *Development* **126**, 5353–5364.
Mandato, CA, and Bement, WM (2001). "Contraction and polymerization cooperate to assemble and close actomyosin rings around *Xenopus* oocyte wounds." *J. Cell Biol.* **154**, 785–797.
Manseau, L, Baradaran, A, Brower, D, Budhu, A, Elefant, F, Phan, H, Philp, AV, Yang, M, Glover, D, Kaiser, K, Palter, K, and Selleck, S (1997). "GAL4 enhancer traps expressed in the embryo, larval brain, imaginal discs, and ovary of *Drosophila*." *Dev. Dyn.* **209**, 310–322.
Martin, P, and Lewis, J (1992). "Actin cables and epidermal movements in embryonic wound healing." *Nature (London)* **360**, 179–183.
Martin, P, and Wood, W (2002). "Epithelial fusions in the embryo." *Curr. Opin. Cell Biol.* **14**, 569–574.
Martinez-Arias, A (1993). "The Development of *Drosophila melanogaster*." Cold Spring Harbor, New York. 517–607 pp.
Millard, TH, and Martin, P (2008). "Dynamic analysis of filopodial interactions during the zippering phase of *Drosophila* dorsal closure." *Development* **135**, 621–626.
Mizuno, D, Tardin, C, Schmidt, CF, and Mackintosh, FC (2007). "Nonequilibrium mechanics of active cytoskeletal networks." *Science* **315**, 370–373.
Mooney, DJ, Langer, R, and Ingber, DE (1995). "Cytoskeletal filament assembly and the control of cell spreading and function by extracellular matrix." *J. Cell. Sci.* **108**, 2311–2320.
Oda, H, and Tsukita, S (2001). "Real-time imaging of cell-cell adherens junctions reveals that *Drosophila* mesoderm invagination begins with two phases of apical constriction of cells." *J. Cell. Sci.* **114**, 493–501.
Peralta, XG, Toyama, Y, Hutson, S, Montague, R, Venakides, S, Kiehart, DP, and Edwards, GS (2007). "Upregulation of forces and morphogenic asymmetries in dorsal closure during *Drosophila* development." *Biophys. J.* **92**, 2583–2596.
Peralta, XG, Toyama, Y, Kiehart, DP, and Edwards, GS (2008). "Emergent properties during dorsal closure in *Drosophila* morphogenesis." *Phys. Biol.* **5**, 15004.
Ridley, AJ (2006). "Rho GTPases and actin dynamics in membrane protrusions and vesicle trafficking." *Trends Cell Biol.* **16**, 522–529.
Roberts, DB (1998). *Drosophila: a practical approach*, IRL Press, Oxford.
Singer, AJ, and Clark, RA. F (1999). "Cutaneous wound healing." *N. Engl. J. Med.* **341**, 738–746.
Smith, NP, Barclay, CJ, and Loiselle, DS (2005). "The efficiency of muscle contraction." *Prog. Biophys. Mol. Biol.* **88**, .
Song, B, Zhao, M, Forrester, J, and McCaig, C (2004). "Nerve regeneration and wound healing are stimulated and directed by an endogenus electrical field in vivo." *J. Cell. Sci.* **117**, 4681–4690.

Wada, A, Kato, K, Uwo, MF, Yonemura, S, and Hayashi, S (2007). "Specialized extraembryonic cells connect embryonic and extraembryonic epidermis in response to Dpp during dorsal closure in *Drosophila*." *Dev. Biol.* **301**, 340–349.

Winter, C, Wang, B, Ballew, A, Royou, A, Karess, R, Axelrod, J, and Luo, L (2001). "*Drosophila* Rho-associated kinase (*Drok*) links frizzled-mediated planar cell polarity signaling to the actin cytoskeleton." *Cell* **105**, 81–91.

Wood, W, Jacinto, A, Grose, R, Woolner, S, Gale, J, Wilson, C, and Martin, P (2002). "Wound healing recapitulates morphogenesis in *Drosophila* embryos." *Nat. Cell Biol.* **4**, 907–912.

Young, PE, Richman, AM, Ketchum, AS, and Kiehart, DP (1993). "Morphogenesis in *Drosophila* requires nonmuscle myosin heavy chain function." *Genes Dev.* **7**, 29–41.